Time-varying effects and averaging issues in models for current-mode control

Citation: Perreault, D.J., and G.C. Verghese. "Time-Varying Effects and Averaging Issues in Models for Current-Mode Control." IEEE Trans. Power Electron. 12, no. 3 (May 1997): 453–461. © 1997 IEEE

As Published: http://dx.doi.org/10.1109/63.575673

Publisher: Institute of Electrical and Electronics Engineers (IEEE)

Persistent URL: http://hdl.handle.net/1721.1/86987

Version: Final published version: final published article, as it appeared in a journal, conference proceedings, or other formally published context

Time-Varying Effects and Averaging Issues in Models for Current-Mode Control

David J. Perreault, *Student, IEEE,* and George C. Verghese, *Senior Member, IEEE*

***Abstract*—This paper investigates issues in modeling of current-mode control. The effects of the current-sampling intrinsic to current-mode control are analyzed, and inadequately recognized limitations of linear time-invariant (LTI) models at high frequencies (where the system behavior is time-varying) are exposed. The paper also examines the geometric methods used to derive duty-ratio constraints in averaged models of current-mode control and points out the sources of discrepancies among various models. The conclusions are supported by simulation and experimental results.**

***Index Terms*—Current-mode control, state-space averaging.**

I. Introduction

MODELING of current-mode-controlled converters has been a topic of interest to the power electronics community for well over a decade. Recently, much effort has been focused on extending the traditional averaged models to capture high-frequency behavior [1]–[4]. Other research has been aimed at improving modeling accuracy by eliminating subtle flaws in the derivation of duty-ratio constraints for current-mode control [5], [6]. This paper (which appeared in a preliminary form as [7]) investigates these recent modeling approaches and, in the process, exposes some serious limitations that have not been adequately accounted for previously. Section II of this paper investigates the impact of sampled data effects on small-signal modeling of current-mode-controlled converters. Section III examines the geometric methods used to derive duty-ratio constraints used for averaged models of current-mode control. The appendix outlines the approach used in our simulations.

Throughout this paper, comparisons between models are made using the boost converter example from [2], shown in Fig. 1. Under normal operating conditions, the switch is turned on every T s and is turned off when the inductor current $i_L(t)$ reaches a peak value of $i_p(t)$ minus a compensating ramp.

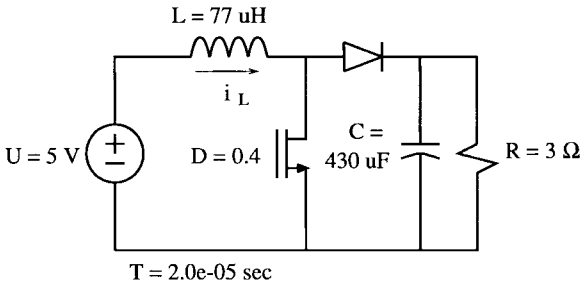

Fig. 1. Example boost converter.

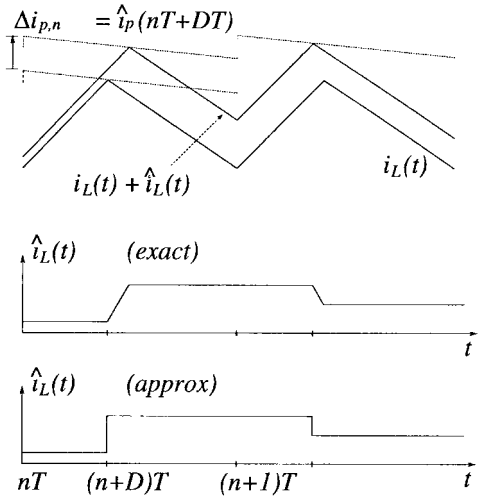

Fig. 2. The approximate sample-and-hold relationship between perturbations in control and peturbations in (instantaneous and average) inductor current.

II. Sampled Data Effects

Efforts to extend small-signal linear time-invariant (LTI) models of current-mode-controlled converters to high frequencies have been motivated by the desire to improve control design, while retaining simplicity. Typically, low-frequency averaged models are used for feedback control design, while a separate high-frequency model is used for slope compensation of the well-known ripple instability. This is done because low-frequency averaged models cannot predict the ripple instability, even under open-loop conditions. On the other hand, models used for predicting subharmonic oscillation do not always capture the behavior of converters operating under closed-loop voltage control. Thus, many researchers have sought to develop LTI transfer functions that fully capture the small-signal behavior of current-mode-controlled converters [1]–[4], [8]. Unfortunately, these works have not sufficiently addressed the limitations imposed by the current sampling intrinsic to current-mode control, leading to results that are subject to misinterpretation.

This section of the paper investigates the effects of current sampling and assesses their impact on control design. As

Manuscript received May 21, 1996; revised February 4, 1997. This work was supported by the Bose Foundation and IEEE Convergence Fellowship in Transportation Electronics.

D. J. Perreault and G. C. Verghese are with the Laboratory for Electromagnetic and Electronic Systems, Massachusetts Institute of Technology, Cambridge, MA 02139 USA.

Publisher Item Identifier S 0885-8993(97)03287-0.

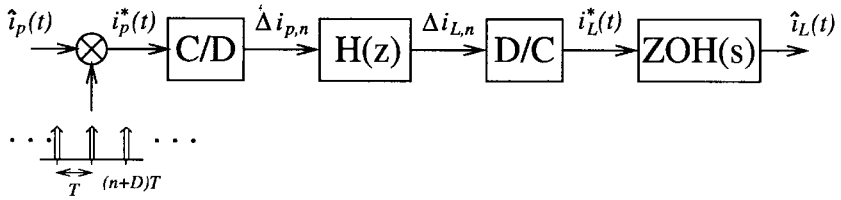

Fig. 3. System for modeling the relation between perturbations in control and perturbations in current. This model relies on the assumptions used in forming $H(z)$.

described in [1] and illustrated in Fig. 2, an approximate sample-and-hold relation exists between a perturbation $\hat{i}_p(t)$ in the control signal $i_p(t)$ and the resulting perturbation $\hat{i}_L(t)$ in inductor current $i_L(t)$ for a current-mode-controlled converter. The corresponding perturbation in the one-cycle *average* inductor current $\hat{i}_L(t)$ is also $\hat{i}_L(t)$, to first order. These facts form the basis for the derivations in [1]–[3] of high-frequency extensions to low-frequency models. A similar approach, expressed in terms of duty-ratio perturbations, is used in [4]. A more exact numerical approach to generating a transfer function is described in [8], but the limitations imposed by current sampling apply equally there as well. What is not made clear in all these works is that, because of the sampling and reconstruction, the system becomes significantly *time varying* (in fact, *periodically* varying) to perturbations in $i_p(t)$ that approach half the switching frequency. This leads to the injection of additional frequencies in $\hat{i}_L(t)$ and thereby causes significant deviations from the results suggested by existing treatments.

A. Modeling Approach

Consider the effect of a perturbation in the control signal $i_p(t)$ of a current-mode-controlled converter. With the assumption that the input and output voltages do not vary significantly, the relation between the perturbation in control and the resulting current perturbation can be approximated by a sample-and-hold system (Fig. 2). That is, the exact current perturbation $\hat{i}_L(t)$ (which is the difference between the transient and steady-state currents) is well-approximated by the zero-order hold (ZOH) of its samples $\Delta i_{L,n}$, taken at the turn-off instants. As discussed in [1], the main effects not modeled by the sample-and-hold approximation are the variation in sampling time and the finite slope of the current perturbation transition. The samples $\Delta i_{p,n}$ of the instantaneous current perturbation can also be seen as approximate samples of the average current perturbation over the ensuing interval of length T. Discrete-time relations can now be formed between the samples $\Delta i_{p,n}$ of the control perturbation and samples $\Delta i_{L,n}$ of the average inductor-current perturbation, as described in [1]. In the small-signal limit, the LTI model of [1]–[3] results, with the z-transform transfer function given by

$$H(z) = \frac{\Delta i_L(t)}{\Delta i_p(z)} = \frac{(m_1 + m_2)z}{(M_c + m_1)z - (M_c - m_2)} \qquad (1)$$

where m_1, m_2, and M_c are the slope magnitudes of the rising inductor current, falling inductor current, and slope-compensation ramp, respectively, in the nominal steady state. (To keep notation streamlined, we employ the same symbol for time-domain and transform-domain quantities, but use the arguments z and s to denote the z and Laplace transforms, respectively.) Under the preceding assumptions, the relation between perturbations in control and perturbations in the average inductor current can then be modeled, as shown in Fig. 3. The impulse modulation represents the sampling action, while the ZOH at the output reconstructs the continuous-time waveform. We use c/d to denote the conversion of an impulse train to a sequence of samples and d/c to denote the inverse operation.

This model has been adopted in [1]–[3] since it predicts how an initial current perturbation will decay and can predict open-loop subharmonic oscillations due to ripple instability, whereas a conventional averaged model cannot. The papers [1]–[3] then attempt to incorporate the sample-and-hold effect into continuous-time LTI models by finding a continuous-time transfer function for the system of Fig. 3. What is ignored in these works is that *the system in Fig. 3 is time-varying for control perturbations approaching half the switching frequency and cannot be described by a transfer function at these frequencies*. That is, the response of the system in Fig. 3 (and the response of current-mode-controlled converters) at these frequencies depends on the position of the control signal, with respect to the sampling points. To see this, note that the sampling process, which is modeled by impulse modulation, generates replicas of the input-frequency spectrum centered at multiples of the sampling (or switching) frequency, $f_{sw} = 1/T$:

$$\hat{i}_p^*(s) = \frac{1}{T} \sum_{n=-\infty}^{\infty} \hat{i}_p\left(s + \frac{2\pi n j}{T}\right). \qquad (2)$$

The effects of the replicas are explicitly ignored in [1]–[3], which make the approximation

$$\hat{i}_s^* \approx \frac{1}{T}\,\hat{i}(s) \qquad (3)$$

to generate a control-to-current transfer function for the system of Fig. 3. (Replica components are also ignored in [4] and [8], although the model derivations are somewhat different.) For low-frequency perturbations, this approximation is justified, since the frequencies generated by the replicas will be well-filtered by the low-pass ZOH reconstruction filter in Fig. 3. However, as can be inferred from the frequency response of the ZOH reconstructor (Fig. 4), the responses due to the replicas will not be well-filtered for higher frequency perturbations. This generates frequency components in the output that were not in the input [9].

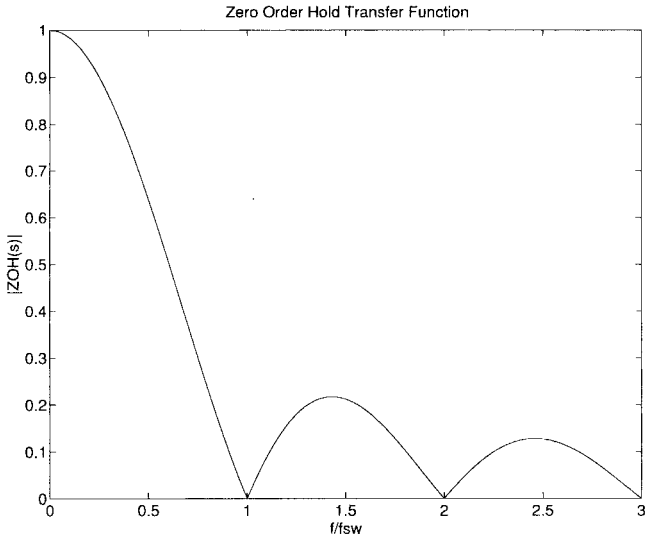

Fig. 4. The frequency response of the ZOH reconstruction filter.

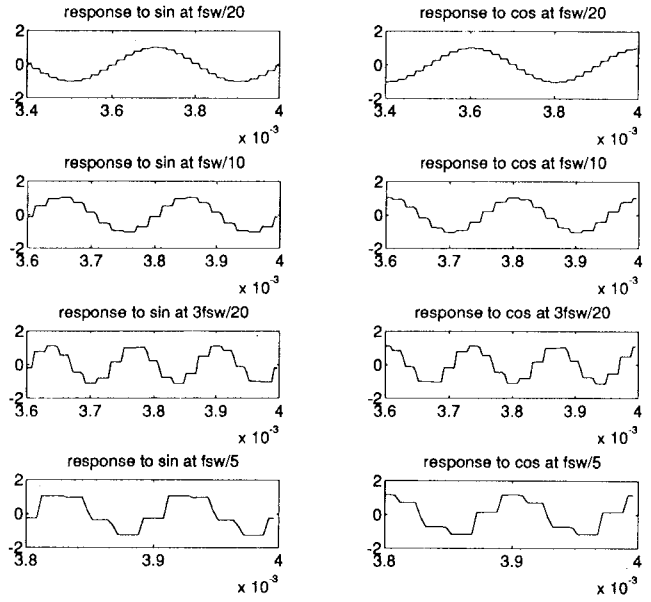

Fig. 5. Small-signal inductor-current response to sinusoidal control perturbations at various frequencies for the converter of Fig. 1 ($I_p = 4.89$ and $M_c = 0$). Response becomes nonsinusoidal above $f_{sw}/10$.

B. Simulation Results

To illustrate the preceding point, the converter of Fig. 1 was simulated for the nominal operating condition corresponding to $D = 0.4$ at $I_p = 4.89$ A and $M_c = 0$, both with and without a small sinusoidal control perturbation at a given frequency. The difference between the inductor currents in the two cases is the small-signal response to the perturbation. As can be seen from the plots in Fig. 5, the response begins to deviate significantly from a sinusoid when the perturbation frequency is within a decade of the switching frequency. Furthermore, differently phased perturbations yield very different results. The frequency components due to the replicas are clearly visible in the waveforms. Similar effects occur in the output-voltage waveforms.

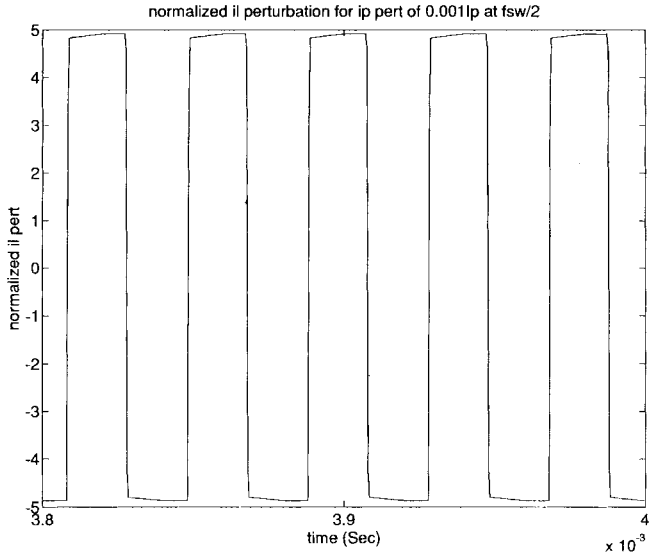

Fig. 6. Small-signal inductor-current response to a control perturbation of amplitude $0.001I_p$ at $f_{sw}/2$ in the boost converter of Fig. 1 ($D = 0.4$ @ $I_p = 4.89$ A and $M_c = 0$). The response is normalized to the amplitude of the perturbation.

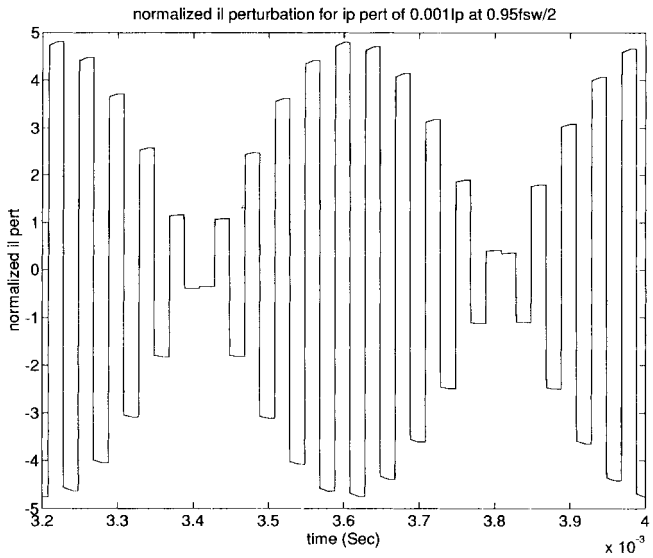

Fig. 7. Small-signal inductor-current response to a control perturbation of amplitude $0.001I_p$ at $0.95f_{sw}/2$ in the boost converter of Fig. 1 ($D = 0.04$ @ $I_p = 4.89$ A and $M_c = 0$). The response is normalized to the amplitude of the perturbation.

What [1]–[4] and [8] have set out to capture is the fundamental component of the response to a sinusoidal perturbation, in effect computing a describing function. This is why predictions in those papers generally agree with narrow-band measurements made using network analyzers. However, models incorporating their approaches are not necessarily reliable for assessing closed-loop stability using LTI design methods. For example, consider the simulated response to a sinusoidal control perturbation at exactly half the switching frequency for the converter of Fig. 1 at the operating condition noted earlier. The amplitude of the perturbation is approximately 0.1% of the nominal $i_p(t) = I_p$, with the

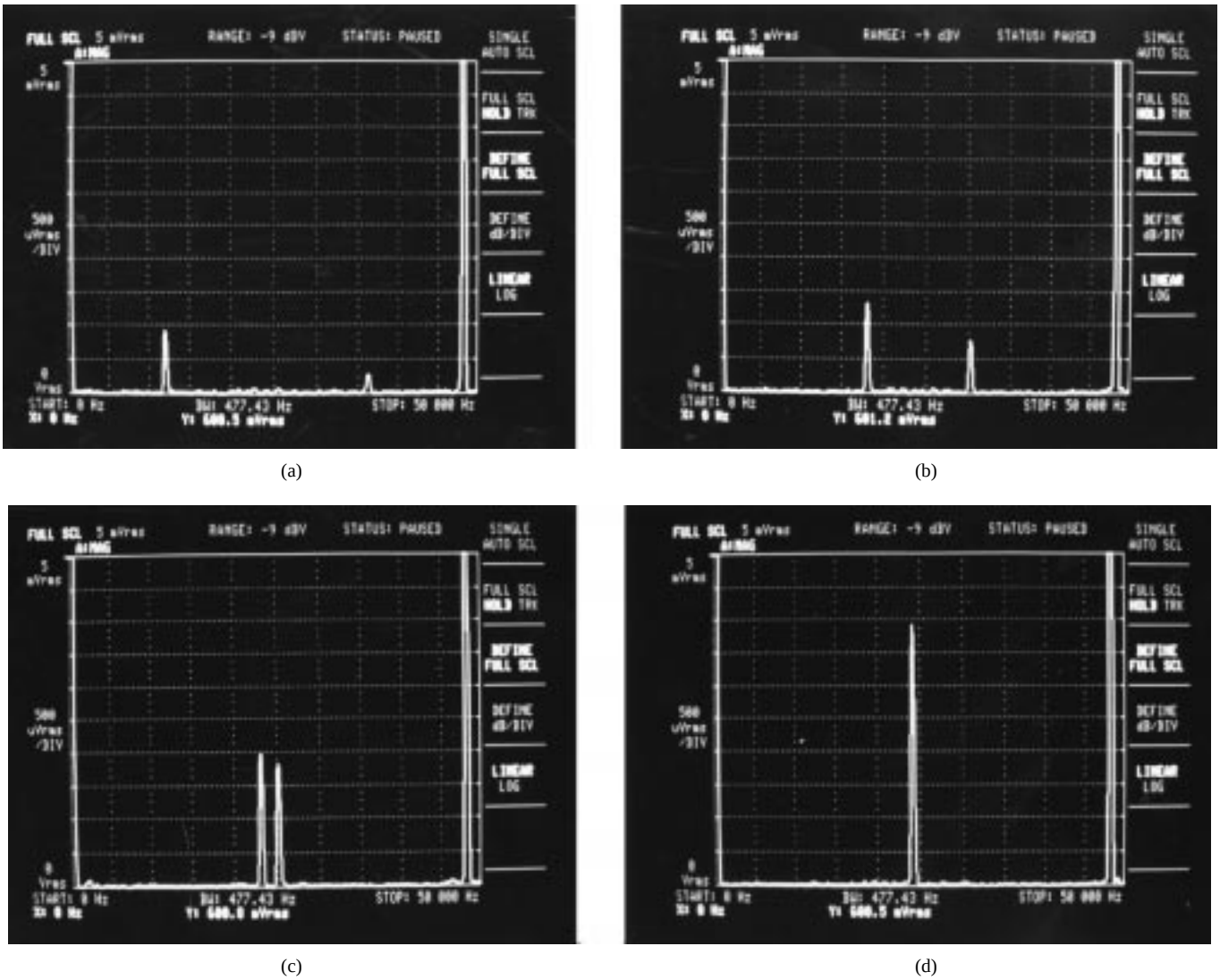

Fig. 8. Inductor-current spectra for sinusoidal control peturbations ($f_{sw} \approx 48$ kHz): (a) 12 kHz, (b) 18 kHz, (c) 23 kHz, and (d) 24 kHz (constructive phase).

describing function of [1]–[3] predicting a control-to-inductor current gain of 3.2. However, because of the superposition of the input signal and one of its replicas at this frequency, the fundamental of the current response to this perturbation (Fig. 6) is approximately *twice as large* as predicted by the describing function of [1]–[3]. (The magnitude of the response plot is normalized to the perturbation magnitude.) The same magnification occurs in the voltage response. Furthermore, the actual small-signal waveform is far from sinusoidal! All of this suggests that there are significant dangers to making frequency-response stability assessments using the LTI model if these assessments depend on LTI model characteristics at frequencies approaching half the switching frequency. Furthermore, the displayed response is for a sine perturbation, with sampling occurring at points $nT + DT$, but differently phased perturbations will yield quite different results. Other interesting effects are also missed by the describing function approach at these frequencies. For example, a sinusoidal perturbation at 0.475 f_{sw} yields output waveforms (Fig. 7), which exhibit strong beating due to the replica at 0.525 f_{sw}.

C. Experimental Results

To demonstrate these effects experimentally, the boost converter of Fig. 1 was constructed. The control circuit built allows one to set a nominal operating point I_p and separately inject an ac perturbation $\hat{\imath}_P(t)$ on top of it. The perturbation signal is capacitively coupled to prevent dc-operating point changes. Monitoring the inductor current with a wideband spectrum analyzer allows all of the frequency components generated by a given perturbation to be observed. Fig. 8 shows the spectrum of the response to small-signal perturbations at different frequencies. The observed responses closely match those predicted by our simulations and the time-varying model of Fig. 3. As half the switching frequency is approached, the replica harmonic components become significant. Clearly, an LTI model is insufficient for describing the system at these frequencies.

What may be concluded from these results is that adding complexity to low-frequency LTI models in an attempt to capture high-frequency behavior may be of limited value for control-loop design. Of course, modeling the sampling and

TABLE I
DUTY-RATIO CONSTRAINTS USED IN VARIOUS CURRENT-MODE CONTROL MODELS FOR THE BOOST CONVERTER

$\hat{d} = \frac{1}{TM_c}(\hat{i}_p - \hat{i}_L) - \frac{D^2 - D'^2}{2LM_c}\hat{u} - \frac{D'^2}{2LM_c}\hat{v}$	[5]
$\hat{d} = \frac{1}{(M_c + \frac{U}{2L})T}[\hat{i}_p - \hat{i}_L - \frac{DT}{2L}\hat{u}]$	[11,12]
$\hat{d} = \frac{2L}{(D' + \frac{2M_cLD'}{U} - D)VT}[\hat{i}_p - \hat{i}_L - \frac{DD'T}{2L}\hat{v}]$	[2,3]
$\hat{d} = \frac{1}{(\frac{U}{L} + M_c)T}[\hat{i}_p - \hat{i}_L - \frac{DT}{L}(1 - \frac{D}{2} + \frac{D'^2}{2D})\hat{u} + \frac{D'^2T}{2L}\hat{v}]$	[1,4]

reconstruction processes may be useful for stability analyses that directly address the time-varying nature of the system. Modeling these processes can also add accuracy to LTI models at frequencies where time-varying effects are unimportant. For example, as will be seen in Section III, the consequences of sampling are apparent in transfer-function phase responses, even below one-tenth the switching frequency. However, it must be emphasized again that, due to the time-varying nature of the system, as half the switching frequency is approached, LTI model predictions are only reliable for frequencies well below half the switching frequency.

III. EVALUATION OF AVERAGED MODEL DERIVATIONS

Large-signal continuous-time averaged models for dc–dc converters are typically expressed in terms of the continuous duty ratio $d(t)$ used to control the converter. Here, $d(t)$ may be defined [10], [13] as the running average over the interval $[t–T, t]$ of the 0–1 switching function $q(t)$ (see Fig. 9). In current-mode control, the duty ratio is implicitly determined by the circuit waveforms. As a result, an additional duty-ratio constraint must be developed to model current-mode-controlled converters. The duty-ratio constraint relates the duty ratio to the control current and state variables of the converter, and its derivation is usually based on the geometry of the inductor-current waveform. This section of the paper examines the geometric methods used to derive duty-ratio constraints for averaged models of current-mode control.

It was pointed out in [5] that geometric derivations of the duty-ratio constraint should be based on transient waveforms and not steady-state waveforms. The large-signal duty-ratio constraint that describes transient behavior of the system should be perturbed to find the small-signal duty-ratio constraint. Steady-state relationships are substituted into the perturbed model as parameters only *after* the perturbed model is formed, [10, Section 13.5].

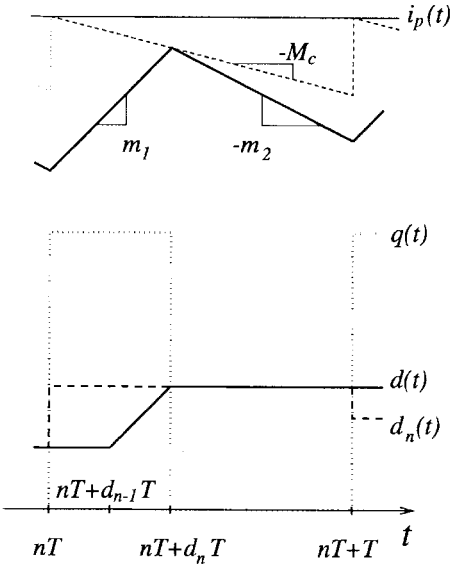

Fig. 9. Inductor-current waveforms for constant-frequency current-mode control, with relationships among $q(t)$, $d(t)$, d_n, $i_L(t)$, and $i_p(t)$.

Consider the geometric evaluation of the duty-ratio constraint, which describes the (local, running) average inductor current $L(t)$ as a function of the continuous duty ratio $d(t)$ and control $\bar{i}_p(t)$. The large-signal duty-ratio constraint is most naturally evaluated over a switching window that coincides with a switching cycle, say $[nT, nT+T]$, so that $d(nT+T) = d_n$ in the notation of Fig. 9. The resulting computation yields

$$\bar{i}_L = i_p - M_c dT - \tfrac{1}{2} m_1 d^2 T - \tfrac{1}{2} m_2 d'^2 T \qquad (4)$$

where $d' = 1-d$. Now, linearize this expression and substitute in the proper waveform slopes for the boost converter, namely

$$\hat{m}_1 = \frac{\hat{u}}{L}, \qquad \hat{m}_2 = \frac{\hat{v} - \hat{u}}{L} \qquad (5)$$

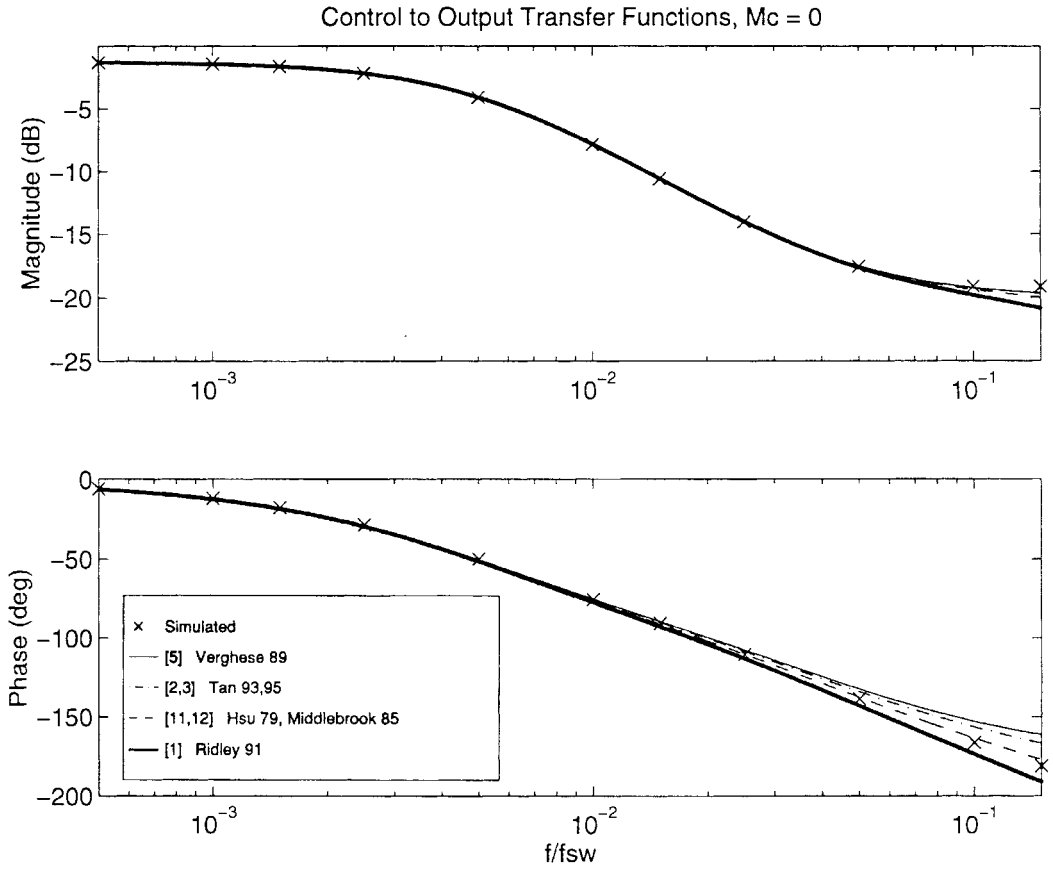

Fig. 10. Small-signal control-to-output frequency responses of various averaged models for the boost converter of Fig. 1 ($D = 0.4$ at $I_p = 4.89$ and $M_c = 0$).

where $u(t)$ and $v(t)$ are the input and output voltages, respectively. This yields the corrected control constraint of [5] (see Table I).

There is, however, an important restriction (not adequately emphasized in [5]) in using (4) as the large-signal constraint. Implicit in the derivation of (4) is the assumption that the average computed over a switching cycle window, such as $[nT, nT+T]$, is representative of the average computed over nearby windows $[nT+\tau, nT+T+\tau]$ and $|\tau| < T$. This assumption effectively limits us to low-frequency variations of the control current.

Many small-signal models [1]–[4], [11], [12] explicitly or implicitly evaluate and reduce the large-signal duty-ratio constraint before the linearization process by substituting in relations that describe the *steady-state* waveforms, such as

$$m_1 d = m_2 d'. \tag{6}$$

Furthermore, depending on how the relations are applied, the papers arrive at different small-signal duty-ratio constraints (Table I). In the conventional method [11], the constraint (6) is applied to (4) before linearizing, yielding

$$\bar{i}_L = i_p - M_c dT - \tfrac{1}{2} m_1 dT. \tag{7}$$

Directly linearizing (7) and substituting in the relations (5) yields the conventional constraint of [11] and [12]. However, if we apply the constraint (6) again, as is done in [2] and [3], we find for the boost converter that

$$m_1 = \frac{u}{L} = \frac{d'v}{L}. \tag{8}$$

Substituting this relation into (7) and linearizing yields the different duty-ratio constraint of [2] and [3]. The papers [1], [4] implicitly assume in their constraint computation that, regardless of the perturbation in duty cycle due to the rising part of the waveform, the inductor current returns to its previous minimum value by the end of the cycle. This constraint is imposed as a consequence of treating the inductor current like a sawtooth modulator waveform in a duty-ratio-controlled converter (which *does* return to the same value at the end of each cycle) and yields yet another duty-ratio constraint.

As it turns out, all of the constraints in Table I lead to essentially the same small-signal LTI model predictions at low frequencies. We offer the following explanation. For low-frequency waveforms, the change in the inductor-current waveform from one cycle to the next is small and, as a result, $m_1 d$–$m_2 d'$ is small. Thus, (6) is a reasonable approximation, and the models all yield similar results.

To see that the low-frequency performance characteristics of the conventional model [11], [12] and the models of [1]–[4] are similar to models based on the corrected approach [5], consider the plots of Figs. 10 and 11, which show the small-signal control-to-current and control-to-output frequency responses for the various models. To separate the issue of correct duty-

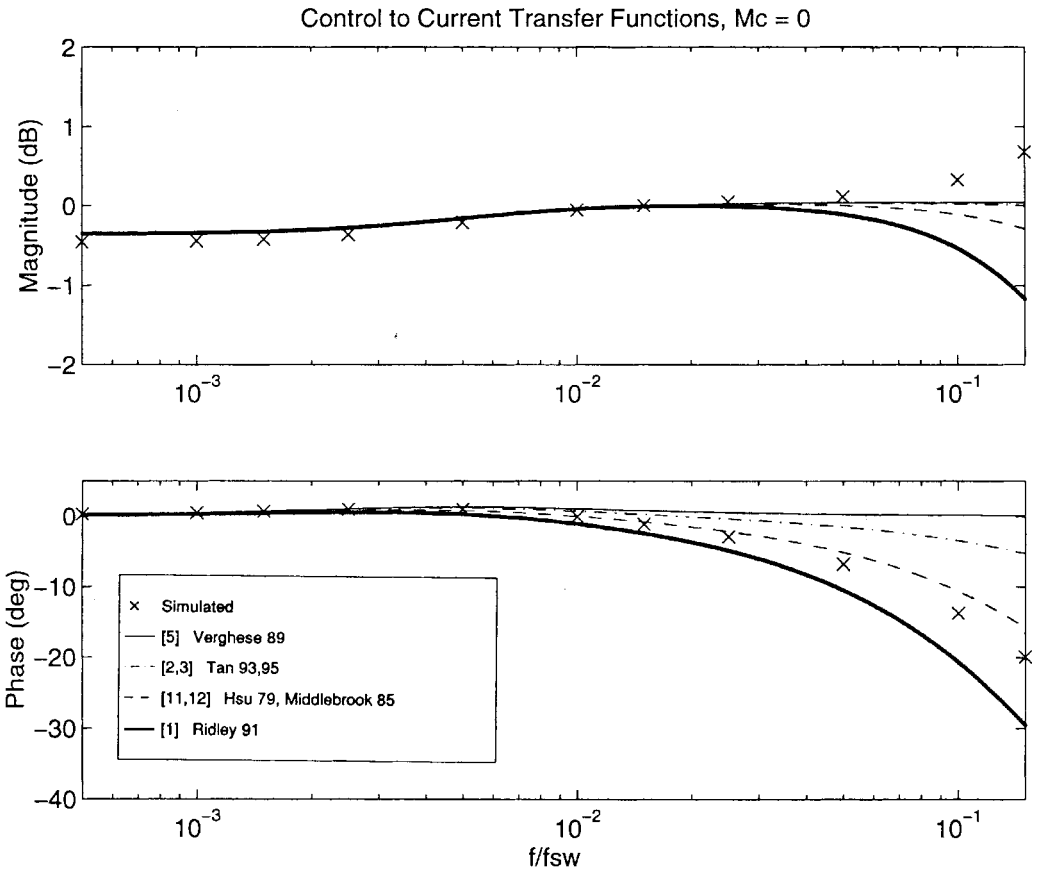

Fig. 11. Small-signal control-to-inductor-current frequency responses of various averaged models for the boost converter of Fig. 1 ($D = 0.4$ at $I_p = 4.89$ and $M_c = 0$).

ratio constraints from the issue of high-frequency modeling addressed in Section II, the additional high-frequency extensions proposed in [1]–[4] have not been incorporated. Samples of the frequency responses determined by simulating the system with and without a perturbation and looking at the difference in response are also plotted. As can be seen, all of these models yield similar results in the magnitude response up to a decade below the switching frequency. There are some differences in the phase responses, even below a tenth of the switching frequency.

It is certainly legitimate to ask how an LTI model may be refined to improve its prediction of the phase characteristic at these *low* frequencies, where the time-varying effects noted in Section II are *not* significant. For instance, as shown in Fig. 12, simply including a phase delay of $\omega T/2$ (the phase response of the ZOH) with the model from [5] yields phase characteristics that much more closely match those computed via simulation (indicated by the crosses). Similarly, the high-frequency extensions proposed in [1]–[4], which are again aimed at capturing the effects of sampling and reconstruction, help to better represent the phase characteristic at lower frequencies.

IV. Conclusion

This paper has looked at several aspects of modeling current-mode-controlled converters. It has been shown that current-mode-controlled converters become significantly time-varying as half the switching frequency is approached. Hence, averaged LTI control models are only reliable for frequencies well below half the switching frequency and are not suitable for predicting subharmonic oscillations due to ripple instabilities.

The geometric methods used to derive duty-ratio constraints have also been examined. It has been confirmed that from a mathematical point of view, duty-ratio constraints should be based on transient waveforms. It is also shown that *both* the conventional and corrected approaches are limited in accuracy when the system deviates significantly from steady state. This leads to similar performance of these models for frequencies at which they can be considered useful. Issues similar to those exposed here for current-mode control may be expected to arise in other contexts, where refinement of averaged models is sought.

Appendix

This appendix details the simulation methods used to calculate the large- and small-signal behavior of current-mode-controlled converters. Calculation of the converter's state trajectory is essentially composed of two tasks. First, the trajectory within a given switch state must be calculated. This trajectory is dependent on the converter topology. Second, the

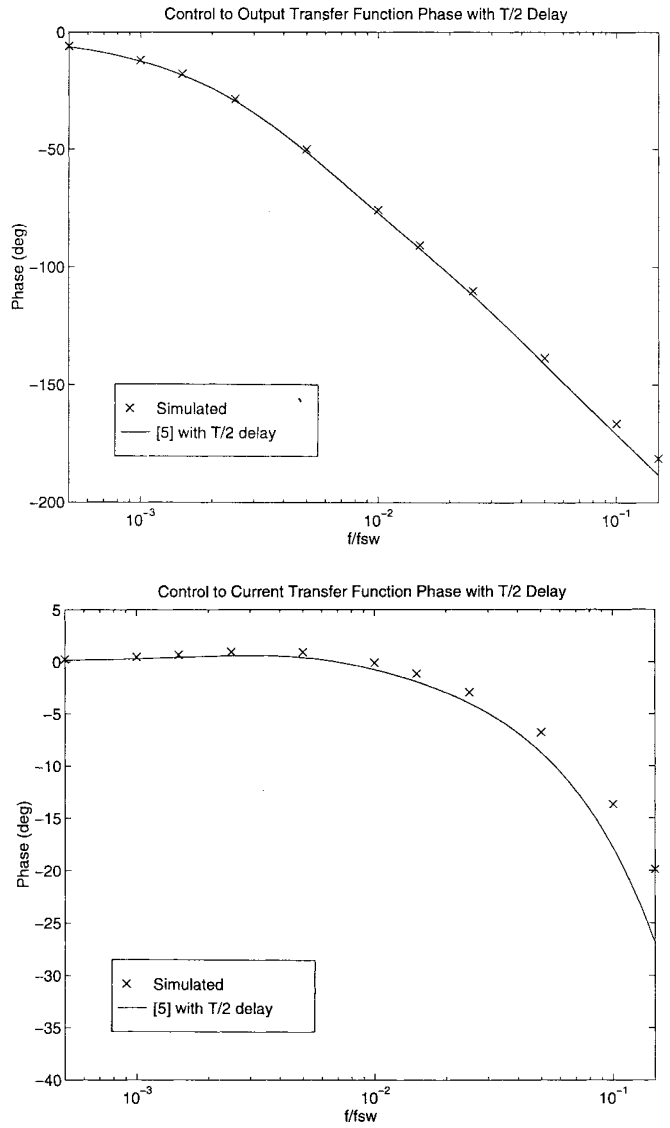

Fig. 12. Small-signal frequency response phases for the corrected model of [5], with an $\omega T/72$ delay to capture the effect of the ZOH. The magnitude responses are unaffected by the delay.

instant of transition between switch states must be found, as specified by the current-mode control law.

Calculation of the trajectories in a given switch state is relatively straightforward for an idealized converter. For the boost converter, the state-space equations describing the system in the transistor on state are

$$\frac{d}{dt}\begin{bmatrix} i_L \\ v \end{bmatrix} = \begin{bmatrix} 0 & 0 \\ 0 & \dfrac{-1}{RC} \end{bmatrix}\begin{bmatrix} i_L \\ v \end{bmatrix} + \begin{bmatrix} \dfrac{1}{L} \\ 0 \end{bmatrix} U. \tag{A1}$$

Solution of this system from t_0 using transform techniques yields

$$\begin{aligned} i_L(t) &= i_L(t_0) + \frac{U}{L}(t - t_0) \\ v(t) &= v(t_0)e^{-(t-t_0)/RC}. \end{aligned} \tag{A2}$$

Similarly, the state-space equations for the diode on state are

$$\frac{d}{dt}\begin{bmatrix} i_L \\ v \end{bmatrix} = \begin{bmatrix} 0 & \dfrac{-1}{L} \\ \dfrac{1}{C} & \dfrac{-1}{RC} \end{bmatrix}\begin{bmatrix} i_L \\ v \end{bmatrix} + \begin{bmatrix} \dfrac{i}{L} \\ 0 \end{bmatrix} U. \tag{A3}$$

When solved from t_0, this yields

$$\begin{aligned} i_L(t) &= A_1 + e^{-\alpha(t-t_0)} \\ &\quad \cdot \{B_1 \sin[\omega_0(t-t_0)] + C_1 \cos[\omega_0(t-t_0)]\} \\ v(t) &= D_1 + e^{-\alpha(t-t_0)} \\ &\quad \cdot \{E_1 \sin[\omega_0(t-t_0)] + F_1 \cos[\omega_0(t-t_0)]\} \end{aligned} \tag{A4}$$

where

$$\begin{aligned} \alpha &= \frac{1}{2RC} \\ \omega_0 &= \sqrt{\frac{1}{LC} - \alpha^2} \\ A_1 &= \frac{U}{R} \\ B_1 &= \frac{\alpha}{\omega_0} i_L(t_0) + \frac{U - V(t_0)}{\omega_0 L} - \frac{\alpha U}{\omega_0 R} \\ C_1 &= i_L(t_0) - \frac{U}{R} \\ D_1 &= U \\ E_1 &= \frac{i_L(t_0)}{\omega_0 C} - \frac{\alpha[U + V(t_0)]}{\omega_0} \\ F_1 &= V(t_0) - U. \end{aligned} \tag{A5}$$

(State equations for other converters may be similarly derived.)

The second task that must be performed is detection of the transition between the two switch configurations. For current-mode control, this occurs when the inductor current rises above the specified threshold. The detection of this transition is accomplished numerically, using a straightforward binary search algorithm. Once the current threshold is exceeded for a given time step, the time step is halved until the transition point is found to the desired resolution.

To calculate the small-signal behavior for a converter at a given operating point, the converter is first simulated without a perturbation (and adjusted to be in steady state for the entire simulation). The converter is then simulated with a sinusoidal perturbation, and the difference is calculated between the two responses. Transfer functions may be constructed by numerically calculating the magnitude and phase of the small-signal response from its samples via a discrete Fourier series computation. The large-signal transient behavior of a converter is simply calculated by repeatedly calling the single-cycle simulator for the desired number of cycles.

ACKNOWLEDGMENT

The authors would like to thank Prof. M. Schlecht and Prof. S. Leeb of MIT for their advice and comments during the course of this research.

REFERENCES

[1] R. Ridley, "A new, continuous-time model for current-mode control," *IEEE Trans. Power Electron.*, vol. 6, no. 2, pp. 271–280, 1991.

[2] F. Tan and R. Middlebrook, "Unified modeling and measurement of current-programmed converters," in *IEEE Power Electron. Specialists Conf.*, 1993, pp. 380–387.

[3] _____, "A unified model for current-programmed converters," *IEEE Trans. Power Electron.*, vol. 10, no. 4, pp. 397–408, 1995.

[4] R. Tymerski and D. Li, "State space models for current programmed pulse width modulated converters," in *IEEE Power Electron. Specialists Conf.*, 1992, pp. 337–344.

[5] G. Verghese, C. Bruzos, and K. Mahabir, "Averaged and sampled-data models for current mode control: A reexamination," in *IEEE Power Electron. Specialists Conf.*, 1989, pp. 484–491.

[6] F. Rodriguez and J. Chen, "A refined nonlinear averaged model for constant frequency current mode controlled PWM converters," *IEEE Trans. Power Electron.*, vol. 6, no. 4, pp. 656–664, 1991.

[7] D. Perreault and G. Verghese, "Time-varying effects in models for current-mode control," in *IEEE Power Electron. Specialists Conf.*, 1995, pp. 621–628.

[8] R. Tymerski, "Application of the time-varying transfer function for exact small-signal analysis," in *IEEE Power Electron. Specialists Conf.*, 1991, pp. 80–87.

[9] G. Franklin, J. Powell, and M. Workman, *Digital Control of Dynamic Systems*, 2nd ed. Reading, MA: Addison-Wesley, 1990, pp. 101–130.

[10] J. Kassakian, M. Schlecht, and G. Verghese, *Principles of Power Electronics.* Reading, MA: Addison-Wesley, 1991.

[11] S. Hsu, A. Brown, L. Rensink, and R. Middlebrook, "Modeling and analysis of switching dc-to-dc converters in constant-frequency current-programmed mode," in *IEEE Power Electron. Specialists Conf.*, 1979, pp. 284–301.

[12] R. Middlebrook, "Topics in multiple-loop regulators and current-mode programming," in *IEEE Power Electron. Specialists Conf.*, 1985, pp. 716–732.

[13] G. Verghese, "Dynamical modeling and control in power electronics," in *The Control Handbook*, W. S. Levine, Ed. Boca Raton, FL: CRC, 1996, pp. 1413–1424.

David J. Perreault (S'91) was born in North Providence, RI, on January 22, 1967. He received the B.S. degree from Boston University, Boston, MA, in 1989 and the S.M. degree from the Massachusetts Institute of Technology (MIT), Cambridge, in 1991, both in electrical engineering.

He is currently a Ph.D. candidate at MIT and a Research Assistant in the MIT Laboratory for Electromagnetic and Electronic Systems, where he is engaged in research and development of cellular power electronic architectures.

Mr. Perreault is a Member of Tau Beta Pi, Sigma Xi, and the National Society of Professional Engineers.

George C. Verghese (S'74–M'78) received the B.Tech. degree from the Indian Institute of Technology at Madras, India, in 1974, the M.S. degree from the State University of New York at Stony Brook in 1975, and the Ph.D. degree from Stanford University, Stanford, CA, in 1979, all in electrical engineering.

Since 1979, he has been at the Massachusetts Institute of Technology (MIT), Cambridge, where he is Professor of Electrical Engineering in the Department of Electrical Engineering and Computer Science and a Member of the Laboratory for Electromagnetic and Electronic Systems. His research interests and publications are in the areas of systems, control, estimation, and signal processing, with a focus on applications in power electronics, power systems, and electrical machines. He is a coauthor (with J. G. Kassakian and M. F. Schlecht) of *Principles of Power Electronics* (Reading, MA: Addison-Wesley, 1991).

Dr. Verghese has served as an Associate Editor of *Automatica*, IEEE TRANSACTIONS ON AUTOMATIC CONTROL, and (currently) IEEE TRANSACTIONS ON CONTROL SYSTEMS TECHNOLOGY. He has served on the AdCom and other committees of the IEEE Power Electronics Society and was also a Founding Chair of its technical committee and workshop on computers in power electronics.